Applied Energy xxx (2017) xxx–xxx

Contents lists available at ScienceDirect

Applied Energy

journal homepage: www.elsevier.com/locate/apenergy

A novel control approach for virtual synchronous generators to suppress frequency and voltage fluctuations in microgrids

Yuko Hirase [a,*], Kensho Abe [a], Kazushige Sugimoto [b], Kenichi Sakimoto [b], Hassan Bevrani [c], Toshifumi Ise [d]

[a] Kawasaki Technology Co., Ltd., Electromechanical System Department, 1-1, Kawasakicho, Akashi, Hyogo 673-8666, Japan
[b] Kawasaki Heavy Industries, Ltd., Electromechanical System Department, 1-1, Kawasakicho, Akashi, Hyogo 673-8666 Japan
[c] University of Kurdistan, Smart/Micro Grids Research Center, Sanandaj 66177-15175, Iran
[d] Osaka University, 2-1, Yamadaoka, Suita, Osaka 565-0871 Japan

HIGHLIGHTS

- The simple algebraic-type VSG provides an intuitive and mathematical comprehension.
- The frequency/voltage deviations caused by parallel operation of SGs are analysed.
- The VSG provides the stabilization effects of the frequency/voltage deviations.
- The analytic approach has good agreement with the simulation/experimental results.
- The VSG promotes the use of renewable energies into the existing power grids.

GRAPHICAL ABSTRACT

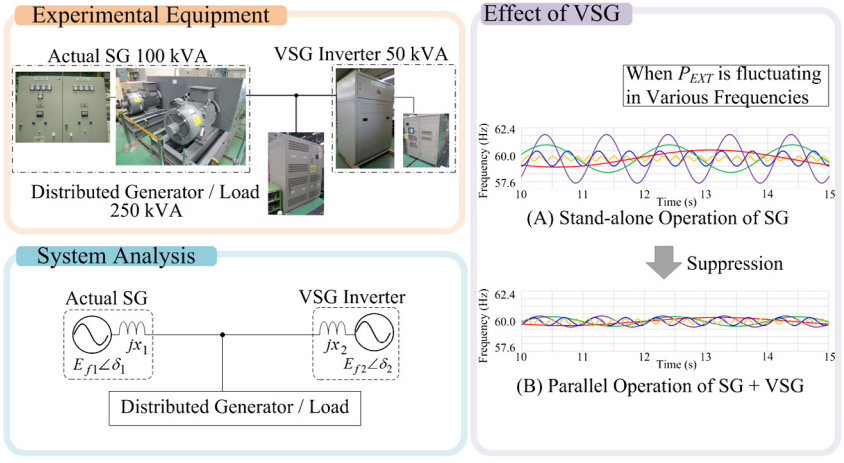

ARTICLE INFO

Article history:
Received 15 February 2017
Received in revised form 15 June 2017
Accepted 16 June 2017
Available online xxxx

Keywords:
Distributed generator
Frequency/voltage deviation
Inverter control
Microgrid
Synchronous analysis

ABSTRACT

To achieve a more sustainable supply of electricity, consumers are expected to rely increasingly on combinations of various types of power generators. Among them, distributed generators (DGs) utilizing renewable energy sources (RESs) are a promising solution. However, introducing renewable energy based DGs into microgrids (MGs) can reduce the inertia of the whole power system, and hence, the system frequency and the voltage can be fluctuated. Furthermore, unnecessary interference occurs as the number of synchronous machines increases. To address these issues, it is desirable to develop a noble inverter control method for DGs, and to gain an intuitive understanding of the dynamic characteristics of MG power systems. In this paper, the impacts of frequency/voltage deviations in MGs are mathematically investigated using algebraic-type virtual synchronous generator (VSG). The algebraic-type VSG with a minimal number of parameters has an ability to suppress the system frequency and voltage deviations. The proposed control approach presents a suitable solution for penetration of more and more renewable energy into the existing power grids. The results of the analysis were verified via simulations and experiments.

* Corresponding author.
E-mail address: hirase-tch@corp.khi.co.jp (Y. Hirase).

http://dx.doi.org/10.1016/j.apenergy.2017.06.058
0306-2619/

1. Introduction

The microgrid (MG) concept has proven to be an appealing alternative for overcoming the challenges of integrating renewable energy sources (RESs) and distributed generators (DGs) into power systems. Although distributed inverter-based power sources have become the main components in MGs, dynamic stability, special protection schemes, and improved control strategies remain the priority. In recent years, the large-scale integration of inverters has created significant challenges for future electric energy systems, including difficulties in achieving frequency stability due to the reduction in system inertia caused by the introduction of inverters with RESs. A general overview of existing MG control technologies and challenges is provided in [1–8]. Protection strategies for the future distribution network are discussed in [1], and a typical residential MG in the near future is predicted in [2]. Utilizing a storage battery with fast responsiveness for frequency stabilization has become popular, and one of which is described in [3]. In [4], a new master-slave DG operation was deployed, and MG-forming model of it is formulated using an advanced optimization method. Nowadays, from the viewpoint of complicated control of centralized control, new decentralized control that replaces centralized control has been studied. In [5], both centralized and decentralized frequency controls are studied, and their advantages and disadvantages are summarized. Furthermore, by boosting use of big data, a research on optimal hierarchical control has been actively carried out in [6–8].

While, in above references, the focus was placed on the control of an MG itself, long-term predictions over wide areas are also being conducted. The United Kingdom (UK) and Ireland have set a goal to increase the introduction rate of RESs up to around 40% by 2020, and are planning to export large amounts of wind power from Ireland to the UK [9]. However, the shortage of system inertia in the power system in Great Britain (GB) was analysed in [10], and the authors of [11,12] warned that the introduction of a large number of RESs in the UK power grid could reduce the inertial constant by up to 70% by 2030.

It has also been proposed that the relevant regulations be strengthen. The British multinational electricity and gas utility company, National Grid plc (NG), is the code administrator for the grid code [13]. To maintain the frequency of the grid within the limits of the statutory range of 49.5–50.5 Hz and the operational range of 49.8–50.2 Hz, each generating unit must satisfy the minimum requirements for response capabilities that have been enacted by NG. Similar regulations have been adopted in several European islands/countries, including the Azores Islands, the Canary Islands, Crete Island, Pantelleria Island, French Islands, and Denmark, and a comparison of these regulations is provided in [14].

As described above, the shortage and reduction of system inertia is an important stability/performance issue in an MG. Detailed analyses of the inertial reduction of MGs and the appropriate countermeasures have also been conducted. In [15], the mechanisms whereby the voltage and frequency of MGs exceed the allowed variation bounds are discussed, and the authors of [16] stated that entire MG systems have lower inertial forces than those in typical commercial grids. In [17], the inertial forces of the wind turbines have been analysed, and a method for applying the associated principles to photovoltaic power generators was introduced. Similarly, since flywheels have rotational energy, their stabilizing effect on MGs has been studied [18,19]. However, because this type of equipment is usually massive and expensive, there is demand for a technique to realize these inertial forces in a pseudo manner using the inverters in DGs. When pseudo inertial forces are realized in a control program, it is called synthetic (virtual) inertia [20–22]. In [10], the frequency control of inverters is governed using a proportional gain and first order element [23]. Although this control method is similar to part of that used in algebraic-type virtual synchronous generators (VSGs) [24], which will be described later, the virtual inertia constant of the controller, reactive power control, and experimental tests were not mentioned in the study. In addition to the above referenced literature, which mostly focus on frequency control, there are also literature that discuss the unstable voltage and other voltage quality problems of MGs. When DGs are introduced into MGs, it leads to collapse of the reactive power balance and decreases the bus voltage [25]. Simulation tests show that voltage stability improves when static synchronous compensators (STATCOMs) and static VAR compensators (SVCs) are added to the grid [26]. Conversely, the problem of frequency fluctuation is not mentioned in these literature.

On the other hand, multiple synchronous generators (SGs) under parallel operation can autonomously suppress frequency/-voltage deviations with their inertial forces and automatic voltage regulators (AVRs). In doing this, they have no need to communicate with either the supervisory controller or each other. In this context, various control systems that enable an inverter to operate like an SG have been studied [24,27–41], and these systems are known as VSGs. Because the software parameters of the frequency/voltage controls can be tuned to enhance the dynamic response of the system, the VSG concept is considered to be a useful solution for improving the resilience of MG systems. Although numerous studies have focused on various types of VSGs, in each case, the VSG simulates the dynamic behaviour of an SG, and represents its fundamental swing equation by virtual inertia, which not only enables the stand-alone operation of a VSG or parallel operation of multiple VSGs, but also enhances the frequency stability of MGs. In [24,27–29], it is proven that VSGs can supply uninterruptable power between grid-connected and islanded operation modes. In addition to the frequency control, VSGs can operate to regulate the system voltage like SGs. Although the effects of voltage stabilization control in VSGs are demonstrated in [30,31], only transient responses have been focused in both research works. What should be noted here is that the consensus-based control, which requires communications among each VSG, is used in [30]. On the other hand, since VSGs have the same function as AVRs of SGs, the communication links are not used in [24,27,28]. A comparison of various VSGs and similar techniques is detailed in [32].

As the authors in [33] have already shown, system instabilities can be exacerbated by the resonance among SGs, DGs, and loads (LDs). That is, as more inverters that have the characteristics of SGs are introduced, the amount of unnecessary interference will be produced. In conventional power grids with SGs, stability analysis procedures were well established for particular classes of problems [34]. However, this may be difficult to achieve and comprehend because the wide range of power technologies were being deployed. Even though the parallel operation of VSGs was studied in [35], there was no focus on entire MG systems, which included VSGs and SGs. Furthermore, manufacturers do not normally disclose detailed device information, such as time constants, control gains, etc. Hence, it is difficult to estimate the influence caused by other equipment in advance and to prepare the necessary compensation countermeasures. Therefore, to minimize unnecessary interference and to construct an intuitive understanding of the dynamic characteristics of an MG, a straightforward design is required. Considering the above, In [33], the authors evaluated a novel two-SG model of an MG, which includes an algebraic-type VSG [24] and a conventional SG, and demonstrated that algebraic-type VSGs could be designed using a minimal number of required parameters. Although only the essential elements of the dynamic characteristics of SGs are applied in algebraic-type

Please cite this article in press as: Hirase Y et al. A novel control approach for virtual synchronous generators to suppress frequency and voltage fluctuations in microgrids. Appl Energy (2017), http://dx.doi.org/10.1016/j.apenergy.2017.06.058

VSG controls, the basic behaviours of a generator can be simulated. The simplicity of algebraic-type VSGs is a benefit when endeavouring to solve the above problems.

In this paper, the conventional SG is assumed the main power supply. In the formulation, both active power (P) - frequency (F) and reactive power (Q) - voltage (V) controls are considered, and they were utilized in the simulation models and experiments. The Q-V control was left as an issue in [33]. Although the P-F and Q-V controls are discussed separately in the mathematical analysis, the results of the analysis are very consistent with those of both the simulation and experiments. It should be noted that the authors presented a preliminary summary of this work in [36].

The remainder of the paper is organized as follows. The characteristics of VSG control are briefly reviewed in Section 2. In Section 3, the dynamics of P-F and Q-V control are discussed, two-machine systems are linearly modelled, and the basic theories of deviation occurrence and suppression for both frequency and voltage are mathematically described. In Section 4, the steady state and frequency responses to sinusoidally oscillating DGs/LDs in MGs are explained through the results of simulation and experiment, and the frequency/voltage suppression effects of VSGs are demonstrated. Hereafter in this paper, the term VSG is used to refer to algebraic-type VSGs.

2. VSG control

Fig. 1 shows the structure of a VSG controlled inverter. Fig. 1(A) shows the connection diagram of a three-phase inverter with VSG control, and Fig. 1(B) shows the corresponding control block diagram [24]. The measured signals are the line-to-line voltages (v_{uv}, v_{vw}) and line currents (i_u, i_w), and v_{PN} represents the voltage of the DC link. The pulse width modulation signals (pwm_u, pwm_v, pwm_w) are calculated in the VSG control and then sent to the bridge inverter. The arrows at the measurement points in Fig. 1 (A) indicate positive directions. The term PLL represents a phase-locked loop.

In this system, the system voltage is measured at the source side of the transformer. The inductor current is also measured, which is used to prevent overcurrent. Although the value of system current at the source side of the transformer is the difference between the current flowing into the filter capacitor and the inductor current, the current in the small filter capacitor is negligible and can be ignored. The inductor current is then equal to the system current.

The generator phase angle (δ) is expressed in radians, and the other variables are expressed in per-unit (pu). The active power (P) is related to the VSG torque and the angular velocity of the rotor (ω_r). The variation in the rotor angular velocity ($\Delta\omega_r$) can be calculated using the portion enclosed by the dashed line box (a) in Fig. 1 (B), which also contains the proportional control gain (K_P) and the first-order lag element of the time constant (T_P). The difference between $\Delta\omega_r$ and the grid angular velocity (ω_g) is added to the reference of the rotor angular velocity (ω_N), and the sum (ω_r) is integrated to produce the generator phase angle (δ).

The magnitude of the reactive power is related to the magnetic field of the VSG. The magnitude of the induced electromotive force (EMF) can be set using a droop constant (K_Q), the first-order lag element of a time constant (T_Q), and the proportional–integral (PI) compensator. The K_Q term is the droop constant of the reactive power and voltage, the first-order lag element indicates a measurement filter, and the PI compensator is a type of AVR (denoted by dashed line box (b) in Fig. 1(B)). Here, the induced EMF vector is denoted as $\mathbf{E_f} = [e_d, e_q]^t$, and $E_f = |\mathbf{E_f}|$ is its magnitude.

The dashed line box marked (c) in Fig. 1(B) is an impedance model. The vector diagram shows the relationship of three vectors: $\mathbf{E_f}$, $\mathbf{V}_g$, and $\mathbf{I}^*$, where $\mathbf{V}_g = [v_d, v_q]^t$ is a grid (inverter-output) voltage vector, and $V_g = |\mathbf{V}_g|$ is its magnitude. $\mathbf{I}^* = [i_d^*, i_q^*]^t$ is an inverter current command vector, and i_d^* and i_q^* are fed to the current feedback control, where the inverter current ($\mathbf{I} = [i_d, i_q]^t$) is regarded as the VSG armature current. The derivation of the vector diagram is represented in (1), where $\mathbf{z} = r + jx$ represents the virtual impedance (r: resistance, x: reactance); and r and x are set in the VSG control program.

$$\begin{bmatrix} i_d^* \\ i_q^* \end{bmatrix} = \boldsymbol{Y}\left(\begin{bmatrix} e_d \\ e_q \end{bmatrix} - \begin{bmatrix} v_d \\ v_q \end{bmatrix} \right)$$
$$\boldsymbol{Y} = \frac{1}{r^2+x^2} \begin{bmatrix} r & x \\ -x & r \end{bmatrix} = \begin{bmatrix} y_{dd} & y_{dq} \\ -y_{dq} & y_{dd} \end{bmatrix} \quad (1)$$

In addition to the virtual impedance, the inverter has the actual impedance of an AC output filter. In the high-frequency range of the AC output filter, the actual impedance is more dominant than the virtual impedance. Conversely, in the low-frequency range around the grid frequency, the virtual impedance is more dominant [24].

From the constructions described thus far, an inverter with a VSG control can have the characteristics of an SG. This will be explained in the following section. However, because our purpose is not to reproduce the detailed behaviour of an SG with an inverter, the VSG is not equipped with other features, such as pseudo damper windings, and so on.

3. Analytical description

In this section, the P-F and Q-V controls are represented in linear models. These assumptions will be validated in Section 4. To simplify the calculations, the resistance r will be neglected because, as was explained in the previous section, it is not significant.

3.1. Active power and frequency (P-F) control

Part (a) in Fig. 1(B) represents the combination of the governor and rotor inertia. The mathematical derivation of the associated dynamics is presented in [33] precisely and will be reviewed briefly here. Before explaining the VSG configuration, we first consider general SG operations, as shown in Fig. 2.

The stand-alone operation of a single SG is illustrated in Fig. 2. Fig. 2(A) shows a connection diagram of a system containing one SG (SG), where P is the output active power, Q is the output reactive power, E_f is the electromotive force, x is the reactance, δ is set from standard point (G_N) to E_f, and ω and ω_N denote the rotor angular velocity and its reference. ω and ω_N are expressed in rad/s, and other variables are expressed in pu. The infinitesimal change of the general swing equation can be represented as (2), where M represents a moment of inertia expressed in seconds, and P_{in} and P_{out} denote the input and output active powers expressed in pu. In this study, small variations are represented using the prefix Δ.

$$\Delta P_{in} - \Delta P_{out} = M(d\Delta\omega/dt) \quad (2)$$

If $H_{gov}(s)$ represents the transfer function of its governor, $\Delta P_{in} = -H_{gov}(s)\Delta\omega$ is satisfied in the Laplace field. Therefore, by rewriting ΔP_{out} as ΔP and setting $G_{PF}(s) = \Delta\omega/\Delta P$, (3) can be derived (Fig. 2(A)).

$$G_{PF}(s) = \frac{\Delta\omega}{\Delta P} = -\frac{1}{Ms + H_{gov}(s)} \quad (3)$$

Generally, $H_{gov}(s)$ can be written most simply as $H_{gov}(s) = K/(1+sT)$, where K with no units indicates the inverse of a droop constant, and T in seconds indicates the engine and

Please cite this article in press as: Hirase Y et al. A novel control approach for virtual synchronous generators to suppress frequency and voltage fluctuations in microgrids. Appl Energy (2017), http://dx.doi.org/10.1016/j.apenergy.2017.06.058

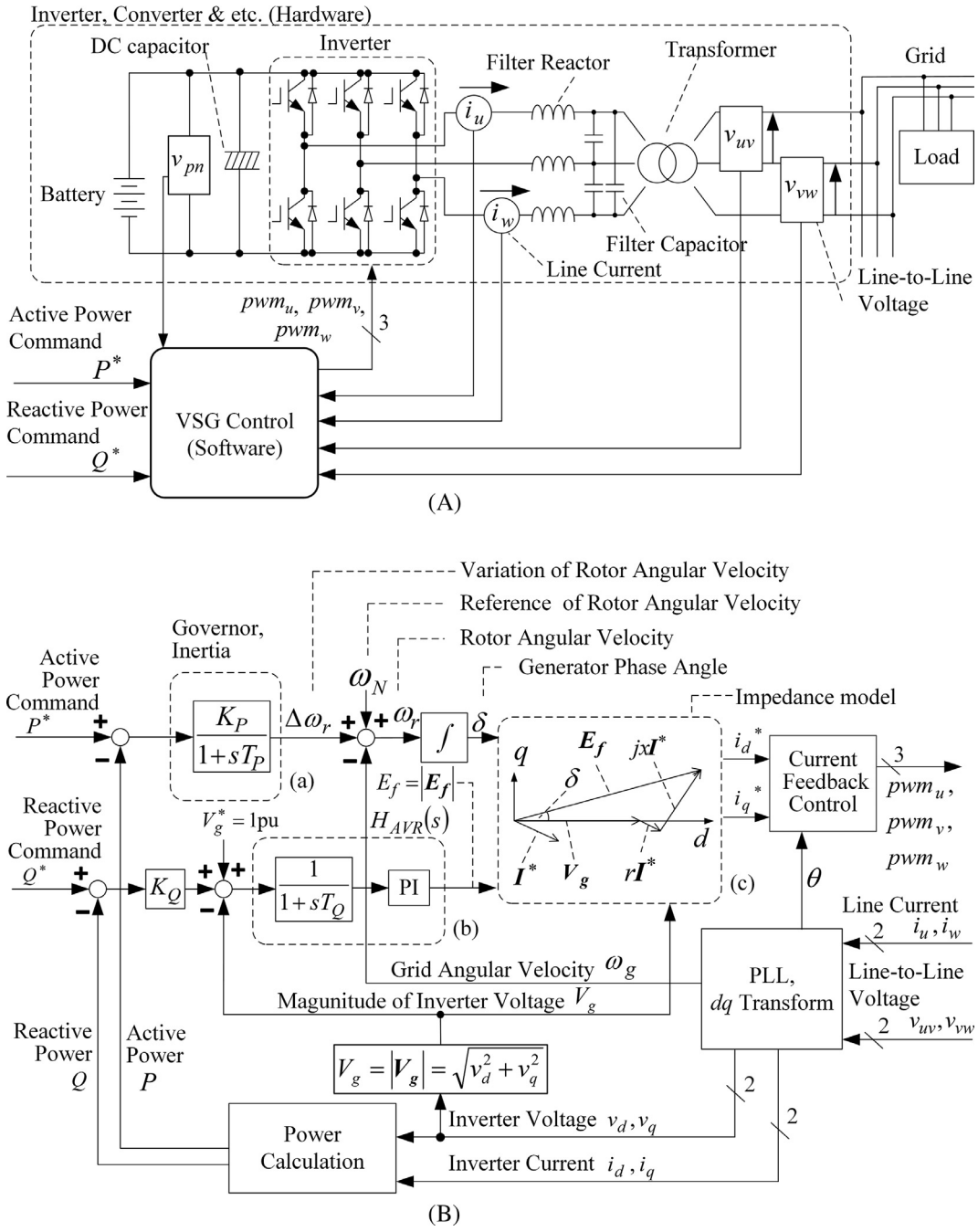

Fig. 1. VSG inverter structure. (A) Connection diagram of three-phase inverter with VSG control. (B) Control block diagram of VSG control.

electrical delays, which certainly exist in actual systems. The result of this expansion is $G_{PF}(s) = -(Ts+1)/(MTs^2+Ms+K)$. In steady state, $G_{PF}(s) = \Delta\omega/\Delta P = -1/K$, which represents a droop characteristic as described in [42]. From these equations, it can be seen that resonance will occur if the power of DGs/LDs fluctuates at a frequency close to the natural frequency $(1/2\pi(K/MT)^{1/2})$, or if other SGs have similar natural frequencies.

Now, the VSG configuration described in Figs. 1 and 2 is reconsidered. Since a software-based VSG created with software has no need to adopt the delays of an actual governor, $G_{PF}(s) = -1/(Ms+K)$ can be obtained by setting $T = 0$. $G_{PF}(s)$ has no resonance frequency, and K_P and T_P in Fig. 1 (B) can be determined using $K_P = 1/K$, $T_P = M/K$. Thus, the VSG can avoid unnecessary interference among the other parallel running machines. Virtual realization is a characteristic advantage of VSG control, which cannot be achieved in actual SGs.

Next, we consider a parallel operation with two SGs (SG_1 and SG_2), as shown in Fig. 2 (B). Multiple SGs with similar systems can be condensed and considered as one SG system. The subscript (n = 1, 2) indicates the respective SG. The units of each parameter are the same as those in Fig. 2(A). The terms P_{EXT} and Q_{EXT} express the active and reactive powers supplied to the DGs/LDs. From (3), the transfer functions $G_{PF1}(s) = \Delta\omega_1/\Delta P_1$ and $G_{PF2}(s) = \Delta\omega_2/\Delta P_2$ can be expressed as (4). Here, $H_n(s)$ (n = 1, 2) are the transfer functions of the governors in SG_1 and SG_2. Each consists of K_n (inverse droop constant), T_n (time constant of governor), and M_n (moment of inertia) (n = 1, 2). If SG_1 is a VSG, $G_{PF1}(s)$ can be rewritten as $G_{PF1}(s) = -1/(sM_1 + K_1)$.

Please cite this article in press as: Hirase Y et al. A novel control approach for virtual synchronous generators to suppress frequency and voltage fluctuations in microgrids. Appl Energy (2017), http://dx.doi.org/10.1016/j.apenergy.2017.06.058

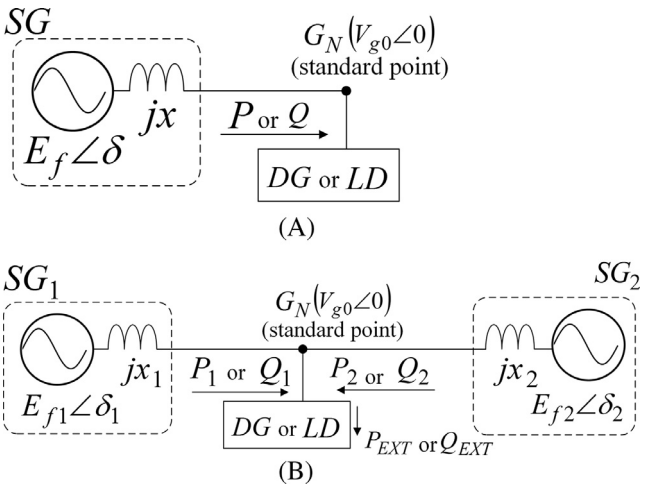

Fig. 2. Connection diagrams of general SGs and DG/LD. (A) Stand-alone operation of a single SG. (B) Parallel operation of two SGs.

$$\begin{cases} G_{PF1}(s) = -\dfrac{1}{sM_1 - H_1(s)} = -\dfrac{sT_1+1}{s^2M_1T_1 + sM_1 + K_1} \\ G_{PF2}(s) = -\dfrac{1}{sM_2 - H_2(s)} = -\dfrac{sT_2+1}{s^2M_2T_2 + sM_2 + K_2} \end{cases} \tag{4}$$

Because the difference between the small variations in δ_1 and δ_2 is given by $\Delta\delta_1 - \Delta\delta_2 = \omega_N \int(\Delta\omega_1 - \Delta\omega_2)dt$, the small variations in P_1 and P_2 are $\Delta P_1 = P_1'\Delta\delta_1$ and $\Delta P_2 = P_2'\Delta\delta_2$, respectively. Here, $P_1' = (E_{f_{10}}V_{g_0}/x_1)\cos\delta_{10}$ and $P_2' = (E_{f_{20}}V_{g_0}/x_2)\cos\delta_{20}$ are known as synchronization forces, and hereafter, subscript 0 represents the initial value of each parameter. Therefore, from the relationship $\Delta P_1 + \Delta P_2 = \Delta P_{EXT}$, ΔP_1 and ΔP_2 can be obtained as (5).

$$\begin{cases} \Delta P_1 = \dfrac{P_1'P_2'}{P_1'+P_2'}\dfrac{\omega_N(\Delta\omega_1 - \Delta\omega_2)}{s} + \dfrac{P_1'}{P_1'+P_2'}\Delta P_{EXT} \\ \Delta P_2 = \dfrac{P_1'P_2'}{P_1'+P_2'}\dfrac{\omega_N(\Delta\omega_2 - \Delta\omega_1)}{s} + \dfrac{P_2'}{P_1'+P_2'}\Delta P_{EXT} \end{cases} \tag{5}$$

From (4) and (5), the transfer function from ΔP_{EXT} to $\Delta\omega_2$ is calculated as (6).

$$\frac{\Delta\omega_2}{\Delta P_{EXT}} = \frac{G_{PF2}(s)}{1 + \left(\frac{1}{P_2'} - \frac{\omega_N}{s}G_{PF2}(s)\right)/\left(\frac{1}{P_1'} - \frac{\omega_N}{s}G_{PF1}(s)\right)} \tag{6}$$

The control block diagrams of (3) and (6) are shown in Fig. 3.

3.2. Reactive power and voltage (Q-V) control

In this section, we analyse *Q-V* control using a mathematical approach rather than a numerical analysis. In the same manner as in the *P-F* control discussion, we first consider the stand-alone operation of a single SG (Fig. 2(A)). The relationship between the reactive power (Q) and the system voltage (V_g) can be written as (7).

$$Q = \frac{E_f V_g \cos\delta - V_g^2}{x} \tag{7}$$

Assuming that the variation of δ is small and $E_{f0}\cos\delta_0 = V_{g0}$, then (8) can be derived from (7).

$$\Delta Q = \frac{V_{g0}^2}{x}\frac{\Delta E_f}{E_{f0}} - \frac{V_{g0}}{x}\Delta V_g \tag{8}$$

Note that this satisfies (9), where $H_{AVR}(s)$ denotes the transfer function of an AVR.

$$\Delta E_f = -H_{AVR}(s)(K_Q\Delta Q + \Delta V_g) \tag{9}$$

Therefore, from (8) and (9), we can derive (10) and (11). The $G_{QV}(s)$ term in (10) represents the transfer function from ΔV_g to ΔQ, and $\bar{G}_{QV}(s)$ in (11) is from ΔQ to $\Delta E_f/E_{f0}$.

$$\frac{\Delta V_g}{\Delta Q} = \frac{1}{G_{QV}(s)} = -\frac{V_{g0}(H_{AVR}(s)/E_{f0})K_Q + x/V_{g0}}{V_{g0}(H_{AVR}(s)/E_{f0}) + 1} \tag{10}$$

$$\frac{\Delta E_f/E_{f0}}{\Delta Q} = \bar{G}_{QV}(s) = \frac{(H_{AVR}(s)/E_{f0})(-K_Q + x/V_{g0})}{1 + V_{g0}(H_{AVR}(s)/E_{f0})} \tag{11}$$

Next, we consider the parallel operation of two SGs (Fig. 2(B)). From (8), the infinitesimal changes of the reactive power in SG_1 and SG_2 are shown as (12).

$$\begin{cases} \Delta Q_1 = (V_{g0}^2/x_1)(\Delta E_{f1}/E_{f10}) - (V_{g0}/x_1)\Delta V_g \\ \Delta Q_2 = (V_{g0}^2/x_2)(\Delta E_{f2}/E_{f20}) - (V_{g0}/x_2)\Delta V_g \end{cases} \tag{12}$$

Then, (13) can be derived from (12) and $\Delta Q_1 + \Delta Q_2 = \Delta Q_{EXT}$.

$$\begin{cases} \Delta Q_1 = \dfrac{V_{g0}^2}{x_1+x_2}\left(\dfrac{\Delta E_{f1}}{E_{f10}} - \dfrac{\Delta E_{f2}}{E_{f20}}\right) + \dfrac{x_2}{x_1+x_2}\Delta Q_{EXT} \\ \Delta Q_2 = -\dfrac{V_{g0}^2}{x_1+x_2}\left(\dfrac{\Delta E_{f1}}{E_{f10}} - \dfrac{\Delta E_{f2}}{E_{f20}}\right) + \dfrac{x_1}{x_1+x_2}\Delta Q_{EXT} \end{cases} \tag{13}$$

From (11), $\bar{G}_{QV1}(s) = (\Delta E_{f1}/E_{f10})/\Delta Q_1$ and $\bar{G}_{QV2}(s) = (\Delta E_{f2}/E_{f20})/\Delta Q_2$ can be obtained from ΔQ_1, ΔQ_2, ΔE_{f1}, and ΔE_{f2}. Based on these equations, (13) can be rewritten as (14).

$$\begin{cases} \Delta Q_1 = \dfrac{V_{g0}^2}{x_1+x_2}(\bar{G}_{QV1}(s)\Delta Q_1 - \bar{G}_{QV2}(s)\Delta Q_2) + \dfrac{x_2}{x_1+x_2}\Delta Q_{EXT} \\ \Delta Q_2 = -\dfrac{V_{g0}^2}{x_1+x_2}(\bar{G}_{QV1}(s)\Delta Q_1 - \bar{G}_{QV2}(s)\Delta Q_2) + \dfrac{x_1}{x_1+x_2}\Delta Q_{EXT} \end{cases} \tag{14}$$

Fig. 4(A) shows the control block diagram of (10) and (11), and Fig. 4 (B) shows that of (14). In the figure, the chained line arrows of Fig. 4 (A) indicate $\bar{G}_{QV}(s)$ and $G_{QV}(s)$.

As shown in Fig. 4(A), the impact from ΔQ to ΔV_g consists of two parts. The dashed line box (a) indicates that the system voltage is influenced by the reactive power through the reactance (x), which allows the reactive power (Q) to suppress the system voltage deviation (ΔV_g). On the other hand, the dashed line box (b) in Fig. 4(A) indicates that the system voltage deviation (ΔV_g) can also be influenced by the droop control (K_Q) and AVR ($H_{AVR}(s)$). The AVR produces the generator voltage (E_f) to suppress the system voltage deviation (ΔV_g).

As shown in Figs. 3(B) and 4(B), the block diagrams of the *P-F* and *Q-V* controls are similar. Fig. 3(B) indicates the impact of the active powers of DG/LD on the system frequency. Fig. 4(B) indicates the impact of the reactive powers of the DG/LD on the system voltage. For this reason, we introduce the transfer functions $\bar{G}_{QVn}(s)$ (n = 1, 2).

The distribution ratios of Q_{EXT} between SG_1 and SG_2 are represented by $G_{QVn}(s)$ (n = 1, 2). From $G_{QV1}(s) = \Delta Q_1/\Delta V_g$, $G_{QV2}(s) = \Delta Q_2/\Delta V_g$, and $\Delta Q_1 + \Delta Q_2 = \Delta Q_{EXT}$, the transfer function from ΔQ_{EXT} to ΔV_g and the distribution ratios of Q_{EXT} between SG_1 and SG_2 are shown as (15) and (16).

$$\frac{\Delta V_g}{\Delta Q_{EXT}} = \frac{1}{G_{QV1}(s) + G_{QV2}(s)} \tag{15}$$

$$\begin{cases} \Delta Q_1 = \dfrac{G_{QV1}(s)}{G_{QV1}(s) + G_{QV2}(s)}\Delta Q_{EXT} \\ \Delta Q_2 = \dfrac{G_{QV2}(s)}{G_{QV1}(s) + G_{QV2}(s)}\Delta Q_{EXT} \end{cases} \tag{16}$$

Please cite this article in press as: Hirase Y et al. A novel control approach for virtual synchronous generators to suppress frequency and voltage fluctuations in microgrids. Appl Energy (2017), http://dx.doi.org/10.1016/j.apenergy.2017.06.058

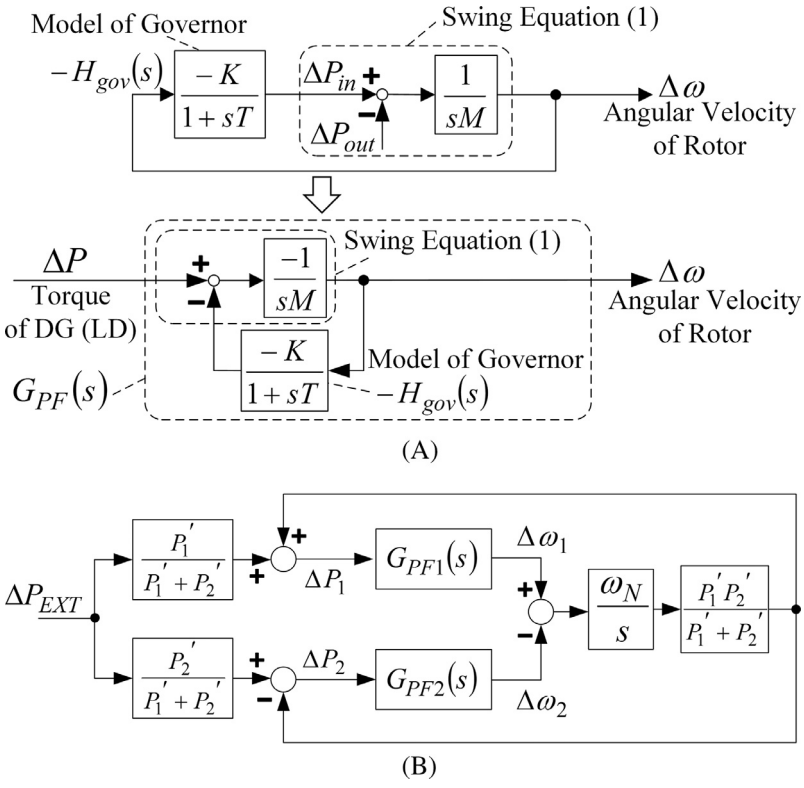

Fig. 3. Control block diagram of active power and frequency control. (A) Stand-alone operation of a single SG (Eq. (3)). (B) Parallel operation of two SGs (Eq. (6)).

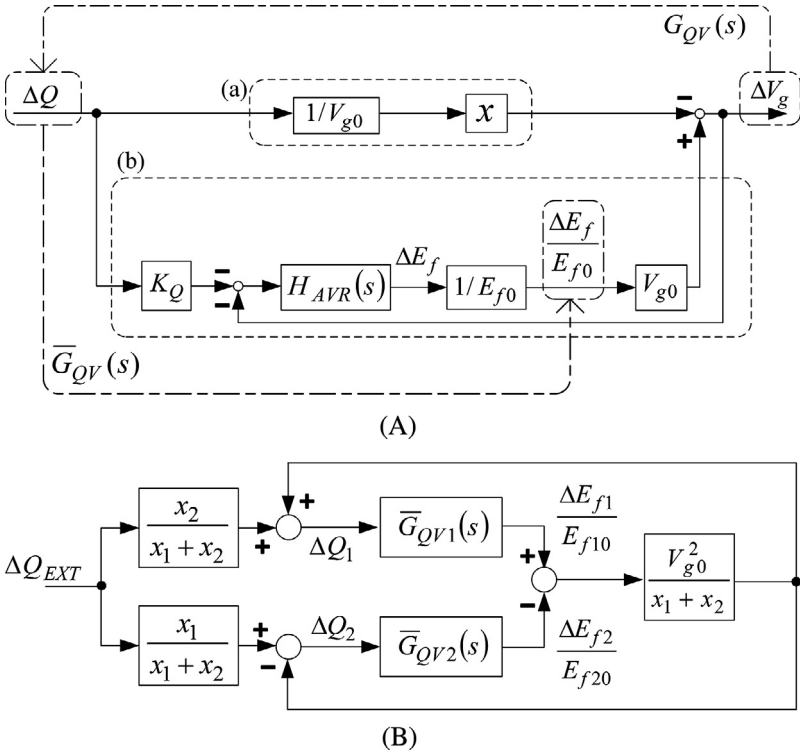

Fig. 4. Control block diagram of reactive power and voltage control. (A) Stand-alone operation of a single SG (Eqs. (10) and (11)). (B) Parallel operation of two SGs (Eq. (14)).

As can be seen in (15), the system voltage deviation from the reactive power deviation greatly depends on $G_{QVn}(s)$ ($n = 1, 2$). From (10), their characteristics are mostly determined by their AVRs ($H_{AVRn}(s)$) and reactances x_n ($n = 1, 2$). If SG_1 is a VSG, as was stated in Section 2, the transfer function of its AVR ($H_{AVR1}(s)$) consists of a noise filter and a PI compensator. On the other hand, if SG_2 is a conventional SG, then it is assumed that SG_2 has a more intricate AVR. For example, the transfer function ($H_{AVR2}(s)$) consists of a measurement filter, PI compensator, proportional–derivative (PD) compensator, exciter output delay element, etc. In the following

Please cite this article in press as: Hirase Y et al. A novel control approach for virtual synchronous generators to suppress frequency and voltage fluctuations in microgrids. Appl Energy (2017), http://dx.doi.org/10.1016/j.apenergy.2017.06.058

section, the AVRs used in the simulation and experimental tests will be detailed.

It is important that the reactances in the *P-F* and *Q-V* controls be carefully assessed. It can be assumed that, under *P-F* control, the impact of the reactance in the low-frequency band is small [33]. Therefore, constant values are assigned to x_1 in P'_1 and x_2 in P'_2 in Fig. 3(B). However, if the *Q-V* control is analysed, it is noteworthy that x_2 in Fig. 4(B) denotes the operational reactance [43], while x_1 is a constant value, as was the case for the *P-F* control. If this was not the case, the results of the theoretical analysis and those of the simulation and experiment would not agree. The specific method used to determine the operational reactance will be discussed in the following section.

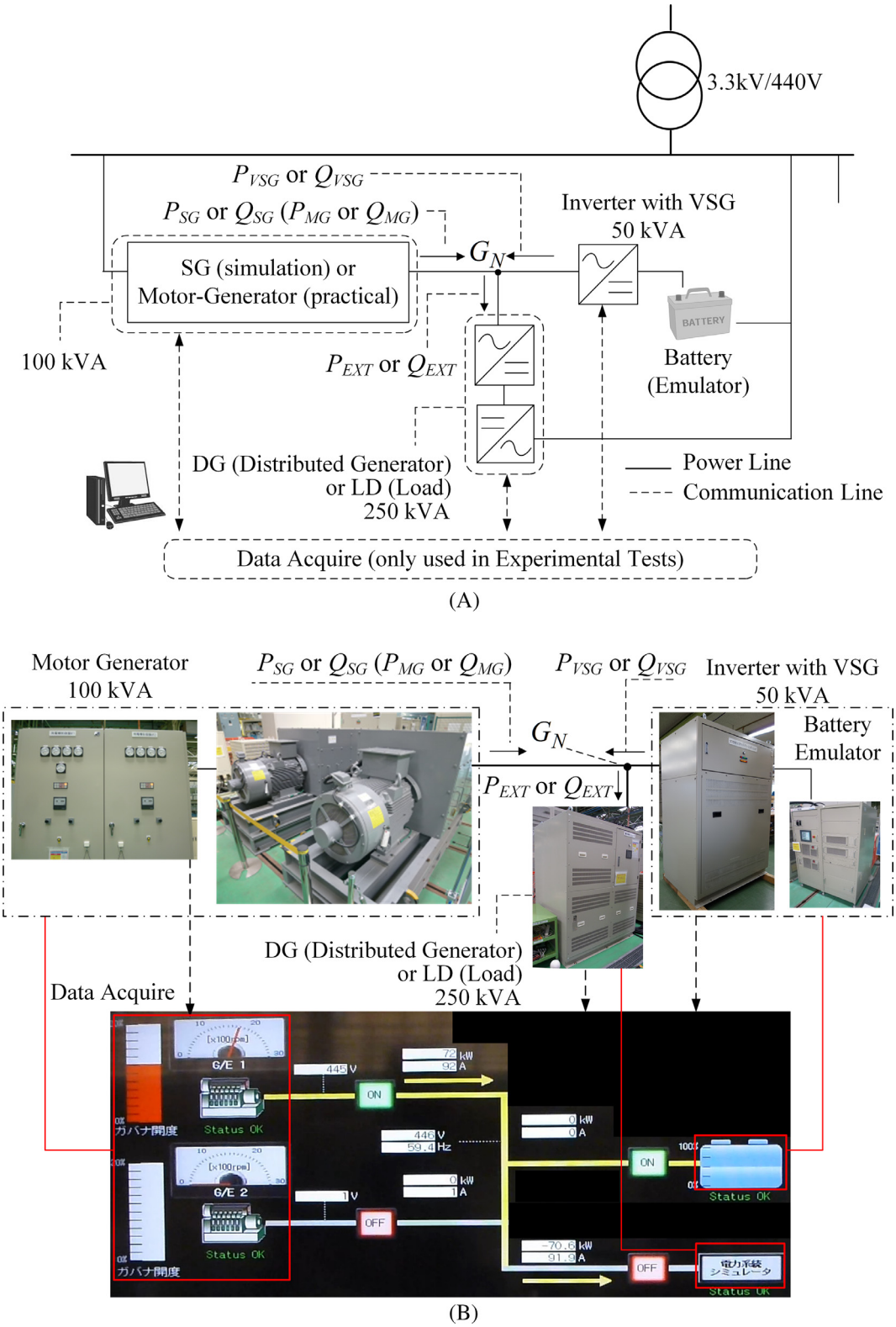

Fig. 5. Test configurations. (A) System diagram of simulation test. (B) Practical system in experimental test (including photographs of the actual machines).

Please cite this article in press as: Hirase Y et al. A novel control approach for virtual synchronous generators to suppress frequency and voltage fluctuations in microgrids. Appl Energy (2017), http://dx.doi.org/10.1016/j.apenergy.2017.06.058

4. Validation by simulation/experimental test results

In this section, the results of the theoretical analysis will be compared with those of the simulations and experiment.

4.1. System configuration

Fig. 5 shows the performed system configuration used for the simulation and experimental tests. The simulator was EMTP-RV Ver. 3.3.0 from POWERSYS, which includes synchronous machine models. In the simulations, test circuits were designed to match the configuration of the actual system used in the experimental tests, as described in the following section.

In the experimental tests, a battery emulator and a motor–generator set were used in place of an actual battery and SG. The motor of the motor–generator set was designed to simulate the characteristics of a conventional diesel engine. The DG/LD was realized by a set of two 250 kW inverters interconnected in the DC portion. The responses of these inverters were sufficiently fast. The switching frequencies of the inverters (i.e., the DG/LD and VSG) were fixes at 8 kHz. The rated frequency was 60 Hz, and the reference of the rotor angular velocity ω_N was $2\pi 60$.

Tables 1 and 2 list the control parameters for the *P-F* and *Q-V* controls in each test case, respectively. Detailed explanations of the parameters are given in [43].

In Cases (a), (b), (c), and (d), the active power of the DG/LD oscillates sinusoidally at frequencies that vary from 0.2 Hz to 5.0 Hz. In Cases (e), (f), (g), and (h), the reactive power oscillates in the same manner. In Cases (a) and (e), the SG_2 (SG or the motor-generator) is operated in stand-alone mode. In Cases (d), (f), (g), and (h), SG_1 acts as a VSG, and runs in parallel with SG_2 (SG or the motor-generator). In Cases (b) and (c), since T_1 does not equal 0, SG_1 is similar to an SG. However, to simplify the calculation, X_{d1}' and X_{d1}'' are not used, and SG_1 is not an exact SG.

In both the theoretical analysis and simulation/experimental tests, constant power is provided by the SG. In the *P-F* analysis tests, constant power of 50 kW is provided before the DG/LD power oscillates. In the *Q-V* analysis tests, constant powers of 50 kW and 20 kVar are also provided in advance. The initial inverter voltage is assumed to be the rated voltage.

As stated in the previous section, the construction of the AVRs and the reactances of SG_1 and SG_2 are determined as follows. If SG_1 is a VSG (Cases (d) and (h)), the transfer function of its AVR ($H_{AVR1}(s)$) consists of a noise filter and a PI compensator. In Fig. 1 (B), T_Q can be considered to have the same value as T_{m1} in Table 2, and $H_{AVR}(s)$ is expressed as (17).

$$H_{AVR}(s) = \frac{1}{1+sT_{m1}}\left(K_{pi1}\left(1+\frac{1}{sT_{i1}}\right)\right) \tag{17}$$

On the other hand, if SG_2 is a conventional SG, it is assumed that SG_2 has an intricate AVR. According to the actual generator used in the experimental tests, the transfer function of SG_2 ($H_{AVR2}(s)$) consists of a measurement filter, a PI compensator, a proportional–derivative

Table 1
Control parameters related to *P-F* control.

	Cases		(a)	(b)	(c)	(d)	(e)	(f)	(g)	(h)
SG_1	Moment of Inertia (M_1)	s	–	1.8	1.0		–		1.0	
	Droop of *P-F* ($1/K_1$)	%	–	5			–		5	
	Time Constant of Governor (T_1)	s	–	0.2		0	–		0	
	Cases		(a)–(h)							
SG_2	Moment of Inertia (M_2)	s	2.0							
	Droop of *P-F* ($1/K_2$)	%	5							
	Time Constant of Governor (T_2)	s	0.3							

Table 2
Control parameters related to *Q-V* control.

	Cases		(a)	(b)	(c)	(d)	(e)	(f)	(g)	(h)
SG_1	Droop of *Q-V* (D_1)	%	–	5			–		5	
	Synchronous Reactance (X_{d1})	pu	–	0.4			–	0.2	0.4	
	Transient Reactance (X_{d1}')	pu	–	–	–	–	–	–	–	–
	Subtransient Reactance (X_{d1}'')	pu	–	–	–	–	–	–	–	–
	Transient time constant in open-circuit (T_{d01}')	s	–	0			–		0	
	Subtransient time constant in open-circuit (T_{d01}'')	s	–	0			–		0	
	Proportional Gain in PI compensator of AVR (K_{pi1})	(–)	–	10			–		10	
	Integral time constant of AVR (T_{pi1})	s	–	0.6			–		0.6	
	Proportional Gain in PD compensator of AVR (K_{pd1})	(–)	–	1			–		1	
	Derivative time constant of AVR (T_{pd1})	s	–	0			–		0	
	Measurement Delay (T_{m1})	s	–	0.005			–	0.01		0.005
	Cases		(a)–(h)							
SG_2	Droop of *Q-V* (D_2)	%	5							
	Synchronous Reactance (X_{d2})	pu	1.01							
	Transient Reactance (X_{d2}')	pu	0.15							
	Subtransient Reactance (X_{d2}'')	pu	0.08							
	Transient time constant in open-circuit (T_{d02}')	s	1.77							
	Subtransient time constant in open-circuit (T_{d02}'')	s	0.02							
	Proportional Gain in PI compensator of AVR (K_{pi2})	(–)	45							
	Integral time constant of AVR (T_{pi2})	s	0.625							
	Proportional Gain in PD compensator of AVR (K_{pd2})	(–)	0.75							
	Derivative time constant of AVR (T_{pd2})	s	0.45							
	Measurement Delay (T_{m2})	s	0.012							

Please cite this article in press as: Hirase Y et al. A novel control approach for virtual synchronous generators to suppress frequency and voltage fluctuations in microgrids. Appl Energy (2017), http://dx.doi.org/10.1016/j.apenergy.2017.06.058

Table 3
Equipment parameters of machines in simulation/experimental tests.

VSG (SG_1)	Cases		(a)	(d)	(e)	(h)
	Rated capacity	kVA	–	50	–	50
	AC voltage of primary	V	–	440	–	440
	AC voltage of secondary	V	–	400	–	400
	DC voltage	V	–	680	–	680
	DC capacitor (smooth)	μF	–	9600	–	9600
	AC reactor (filter)	μH	–	954.5	–	954.5
	AC Capacitor (filter)	μF	–	75	–	75
SG or motor–generator (SG_2)	Cases		(a), (d), (e), (h)			
	Rated capacity	kVA	100			
	AC voltage	V	440			
LD or DG	Cases		(a), (d), (e), (h)			
	Rated capacity	kW	250			
	AC voltage	V	440			

(PD) compensator, and an exciter output delay element. The parameters are listed in Table 2, and $H_{AVR2}(s)$ can be expressed as (18).

$$H_{AVR2}(s) = \frac{1}{1+sT_{m2}}\left(K_{pi2}\left(1+\frac{1}{sT_{i2}}\right)\right)\left(K_{pd2}\frac{1+sT_{d2}}{1+\frac{sT_{d2}}{6}}\right)\frac{1}{1+sT'_{d02}} \quad (18)$$

Furthermore, in the analysis of the *P-F* control, x_1 in P'_1 and x_2 in P'_2 in Fig. 3(B) were set to constant values ($x_1 = X_{d1}$ and $x_2 = X_{d2}{}'$). On the other hand, if the *Q-V* control is analysed, it is noteworthy that x_2 in Fig. 4(B) denotes the operational reactance [43], while x_1 is a constant value ($x_1 = X_{d1}$), as in the *P-F* control. Otherwise, the previous theoretical analysis would not agree with the simulation and

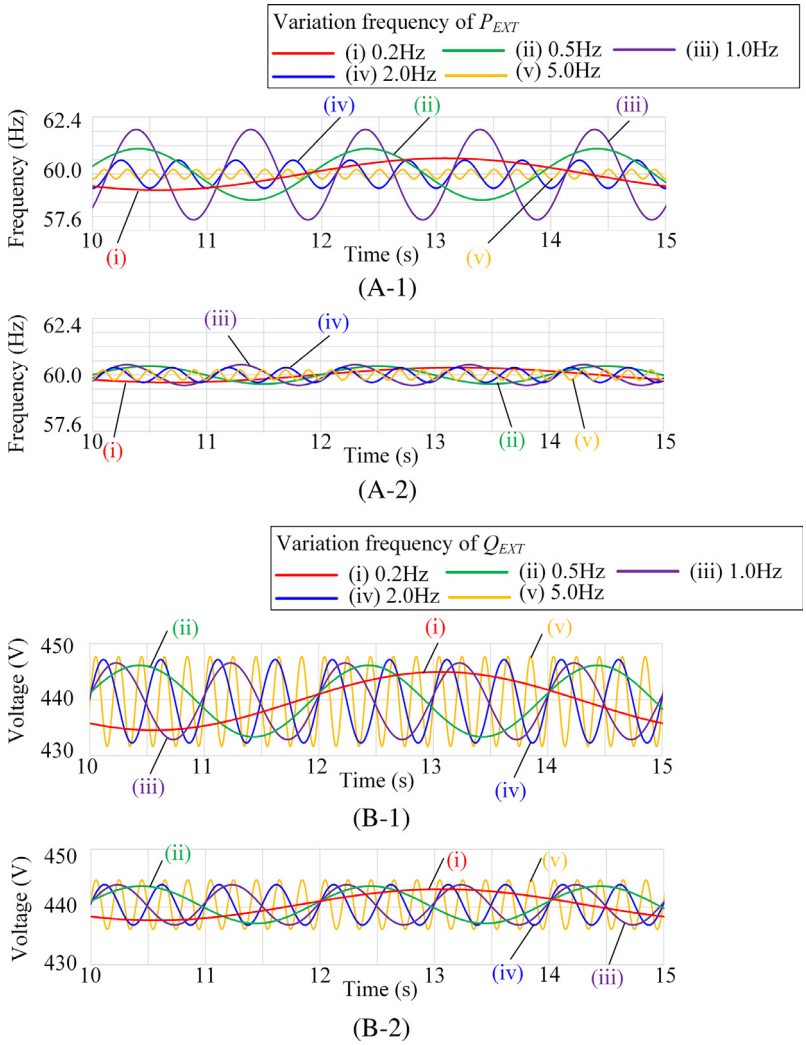

Fig. 6. Simulation results of system frequency and voltage deviations when P_{EXT} and Q_{EXT} oscillates sinusoidally, where their oscillation frequencies vary from 0.2 Hz to 5.0 Hz. (A-1), (B-1) Stand-alone Operation of SG (Cases (a) and (e) in Tables 1 and 2). (A-2), (B-2) Parallel Operation of SG and VSG (Cases (d) and (h) in Tables 1 and 2).

Please cite this article in press as: Hirase Y et al. A novel control approach for virtual synchronous generators to suppress frequency and voltage fluctuations in microgrids. Appl Energy (2017), http://dx.doi.org/10.1016/j.apenergy.2017.06.058

experimental test results. Note that x_2 can be calculated as (19), and that, in Table 2, all the reactance values are saturated values.

$$x_2 = X_{d2}\frac{\left(1+sT'_{d02}\frac{X_{d2}'}{X_{d2}}\right)\left(1+sT''_{d02}\frac{X_{d2}''}{X_{d2}'}\right)}{(1+sT'_{d02})(1+sT''_{d02})} \quad (19)$$

In addition to the control parameters, Table 3 lists the equipment parameters, which need to be selected in the simulation models and experimental equipment. The simulation/experimental tests are only provided in Cases (a), (d), (e), and (h), where the control parameters are equivalent to those of in Tables 1 and 2. Here, the virtual reactance of the VSG (r) is set to 0.2. When the rated capacity of the VSG is converted into 100 kVA, the circuit constants and control parameters become almost equivalent to those of the SG.

4.2. System frequency/voltage deviations (steady-state responses)

Fig. 6 shows the results of simulating the problems in recent MGs and the effects of VSGs. During the simulation, the following frequencies were used for P_{EXT} and Q_{EXT}: (i) 0.2 Hz, (ii) 0.5 Hz, (iii) 1.0 Hz, (iv) 2.0 Hz, and (v) 5.0 Hz. Fig. 6(A-1) and (B-1) show Cases (a) and (e), respectively (stand-alone operations of SG), and Fig. 6 (A-2) and (B-2) show Cases (d) and (h), respectively (parallel operations of SG and VSG).

From Fig. 6(A-1), a ±20 kW deviation of SG_2 should lead to a frequency deviation of ∓0.6 Hz in steady state under the following conditions: *P-F* droop of 5%, rated capacity of 100 kVA, and rated frequency of 60 Hz. Indeed, the frequency varies around ∓0.6 Hz in Case (i) (at the low variation frequency). However, in Cases (iii) and (iv), it varies ∓2.4 Hz. This shows the impact of the active power deviation on the system frequency. In Cases (iii) and (iv) of Fig. 6(A-2), the effect of suppressing the frequency deviation can be seen, and the deviation is almost as much as the estimated value, which is ∓0.3 Hz in steady state under the parallel operation of an SG and a VSG with the same capacity (100 kVA).

The ±20 kVar deviation of SG_2 leads to a theoretical voltage deviation of ∓4.4 V, under the following conditions: *Q-V* droop of 5%, rated capacity of 100 kVA, and rated voltage of 440V. However, in Fig. 6(B-1), it can be seen to vary by almost ∓8.0 V. Although no outstanding effects of the VSG were observed as in suppressing the frequency deviation, Fig. 6(B-2) demonstrates that parallel operation of the SG and VSG can suppress the voltage deviation to the theoretical value of ∓4.4 V without any harmful effects.

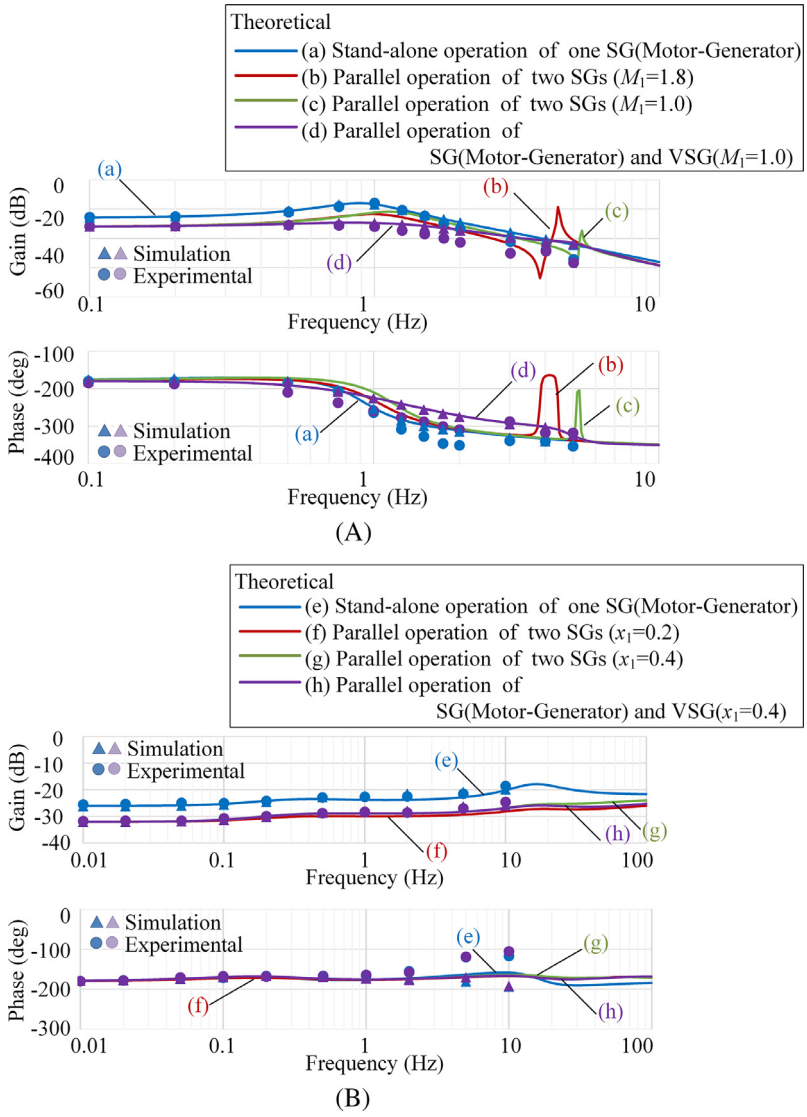

Fig. 7. Frequency characteristics in the simulation and experimental tests, overlaid on graph of theoretical formulas. (A) Frequency characteristics (from ΔP_{EXT} to $\Delta\omega_2$). (B) Frequency characteristics (from ΔQ_{EXT} to ΔV_g).

Please cite this article in press as: Hirase Y et al. A novel control approach for virtual synchronous generators to suppress frequency and voltage fluctuations in microgrids. Appl Energy (2017), http://dx.doi.org/10.1016/j.apenergy.2017.06.058

Based on the results shown in these figures, it is clear that the VSG is able to suppress both frequency and voltage deviations, effectively.

4.3. Frequency characteristics analysis using bode diagrams

Fig. 7(A) and (B) show the frequency responses of the *P-F* and *Q-V* controls, respectively. In the theoretical analysis that was based on the parameters in Tables 1 and 2, the *P-F* and *Q-V* controls were calculated from (6) and (15), respectively. The theoretical characteristics were derived from (6), and they are depicted as the solid lines in Fig. 7(A). Similarly, from (15), the characteristics are shown in Fig. 7(B). In the simulation and experimental tests, they were only calculated from the test results of Cases (a), (d), (e), and (h). The simulation and experimental test results were obtained using a Fourier transform method, and plotted using triangle and dot indicators, respectively. It can be seen in the figures that these indicators frequently overlap.

Theoretically, a frequency deviation of 0.6 Hz in the stand-alone operation of Case (a) is almost equivalent to a gain of $20 * \log(0.6\text{ Hz} / (20\text{ kW} / 100\text{ kW} * 60\text{ Hz}) = -26$ dB. In the parallel operation of Case (d), the gain must be −32 dB. From Fig. 7 (A), the system frequency fluctuations of Cases (a)–(c) were greater than the above assumptions when the load fluctuated at around 1 Hz (Case (a): −16 dB, Case (b): −20 dB, Case (c): −21 dB). Moreover, strong peaks can be seen in the gain curves of Cases (b) and (c) at around 5 Hz (Case (b): −18 dB, Case (c): −34 dB). These results show that resonance appeared among the DG/LD and two machines. However, no significant resonance was observed in Case (d), and the gain was almost −32 dB up to approximately 1 Hz. This was because there was no need to consider the delay time of the virtual governor in the VSG. Precise observations are described in [33].

Similarly, good agreement is observed between the theoretical analysis and the test results in Fig. 7(B). Similar to the above consideration, the test results show that the voltage deviations in a stand-alone operation (Case (e)) and parallel operations (Cases (f)–(h)) were almost equivalent to the theoretical values of −26 dB and −32 dB. As shown in (19), the operational reactance, which can be a destabilizing factor in the system, is closely related to the delay elements that actually exist in the device. However, in the VSG, the virtual impedance is easily modelled because there is no need to realize the exciter delays. Along with the virtual inertia (governor), the virtual impedance is also a characteristic advantage of VSG control. For frequencies larger than 1 Hz, the experimental test results differ from those of the analytical and simulation, due to the measurement method.

Although the *P-F* and *Q-V* controls were discussed separately in the mathematical analysis, the analytic approach was in good agreement with the results of both the simulation and experimental tests. During the testing, both the *P-F* and *Q-V* controls were present in the simulation models and equipment. That is, our results demonstrate that it is feasible to design *P-F* and *Q-V* controls under these conditions independently.

Some of the conducted experimental tests were recorded in Video 1, which is available as the supplementary material.

5. Conclusion

In this paper, the dynamics of the frequency and voltage deviations caused by parallel operation of SGs are analysed, and the stabilization effects provided by VSGs are confirmed. In addition, the simplicity of algebraic-type VSGs provides an intuitive and mathematical comprehension. Although only the essential elements of the dynamic characteristics of an SG are applied in an algebraic-type VSG control, our results demonstrated that those elements are sufficient and their simplicity is necessary to suppress frequency/voltage deviations autonomously. The autonomous suppression can be realized even in a complex MG composed of various devices for which the detailed control methods are not available. Furthermore, it was shown to be feasible to design *P-F* and *Q-V* controls in a single controller independently. This was verified by conducting a theoretical analysis, simulations, and experimental tests under specific conditions.

Although the mutual interference between the *P-F* and *Q-V* controls were shown to be negligible in certain cases, it is essential to have a mathematical grasp of the entire system, in which both controls are considered simultaneously. As part of our future work, our next challenge is to derive mathematical expressions that describe the entire system to clarify under what constraints the interference can be reduced. In this study, it was assumed that multiple SGs with similar systems could be condensed into a single SG system. Thus, another future challenge is to derive a more detailed reduction method that does not impair our intuitive insight.

On the other hand, algebraic-type VSGs have flexible features to supply uninterruptible power between grid-connected and islanded operation modes. In the islanded operation, the VSGs can easily operate in parallel with other types of synchronous machines, such as conventional SGs and other types of VSGs with virtual inertial forces. Because of their flexibility, algebraic-type VSGs are applicable to various areas of MGs. For example, they can be used as the main power generators for individual houses, public offices, disaster prevention facilities, hospitals, factories, various types of bases, college campus, isolated islands, etc.

As was the theme of this paper, interference tends to occur among DGs/LDs in practical applications. For instance, in factories, bases, and isolated islands, frequency and voltage fluctuations are caused by the large pulsed power of LDs, which will lead to the breakage of other equipment connected to the same MGs. Although increasing the rate at which SGs are introduced is a simple way to stabilize the system, the introduction rate of SGs should be limited to maintain their operational efficiency. Furthermore, the economic efficiency drops when fuel must be transported to isolated islands. Therefore, in such situations, using VSGs, which positively affects the frequency/voltage stability and performance, promotes the introduction of RESs in power systems and MGs.

Acknowledgement

This research did not receive any specific grants from funding agencies in the public, commercial, or not-for-profit sectors.

Appendix A. Supplementary matrerial

Supplementary data associated with this article can be found, in the online version, at http://dx.doi.org/10.1016/j.apenergy.2017.06.058.

References

[1] Mandidereza PT, Bansal R. Renewable distributed generation: the hidden challenges – A review from the protection perspective. Renew Sustain Energy Rev 2016;58:1457–65.
[2] Hebner R. The power grid in 2030. IEEE Spectr 2017;54:50–5.
[3] Aghamohammadi MR, Abdolahinia H. A new approach for optimal sizing of battery energy storage system for primary frequency control of islanded Microgrid. Int J Electr Power Energy Syst 2014;54:325–33.
[4] Ding T, Lin Y, Bie Z, Chen C. A resilient microgrid formation strategy for load restoration considering master-slave distributed generators and topology reconfiguration. Appl Energy 2017;199:205–16.
[5] Dehghanpour K, Afsharnia S. Electrical demand side contribution to frequency control in power systems: a review on technical aspects. Renew Sustain Energy Rev 2015;41:1267–76.
[6] Olivares DE, Mehrizi-Sani A, Etemadi AH, Canizares CA, Iravani R, Kazerani M, et al. Trends in Microgrid Control. IEEE Trans Smart Grid 2014;5:1905–19.

Please cite this article in press as: Hirase Y et al. A novel control approach for virtual synchronous generators to suppress frequency and voltage fluctuations in microgrids. Appl Energy (2017), http://dx.doi.org/10.1016/j.apenergy.2017.06.058

[7] Rajesh KS, Dash SS, Rajagopal R, Sridhar R. A review on control of ac microgrid. Renew Sustain Energy Rev 2017;71:814–9.
[8] Mahmoud MS, Alyazidi NM, Abouheaf MI. Adaptive intelligent techniques for microgrid control systems: a survey. Int J Electr Power Energy Syst 2017;90:292–305.
[9] Cleary B, Duffy A, Bach B, Vitina A, O'Connor A, Conlon M. Estimating the electricity prices, generation costs and CO_2 emissions of large scale wind energy exports from Ireland to Great Britain. Energy Policy 2016;91:38–48.
[10] Teng F, Mu Y, Jia H, Wu J, Zeng P, Strbac G. Challenges on primary frequency control and potential solution from EVs in the future GB electricity system. Appl Energy 2017;194:353–62.
[11] Electricity Ten Year Statement (ETYS). Available online at ⟨http://www2.nationalgrid.com/UK/Industry-information/Future-of-Energy/Electricity-ten-year-statement/⟩; 2016 [accessed 17.04.20].
[12] UK Future Energy Scenarios. Available online at ⟨http://fes.nationalgrid.com/media/1195/stakeholder-feedback-document-fes-2017.pdf⟩; 2017 [accessed 17.04.20].
[13] NG. National Grid: Mandatory Frequency Response. Available online at ⟨http://www2.nationalgrid.com/uk/services/balancing-services/frequency-response/mandatory-frequency-response/⟩; 2016 [accessed 17.04.20].
[14] Rodrigues EMG, Osório GJ, Godina R, Bizuayehu AW, Lujano-Rojas JM, Catalão JPS. Grid code reinforcements for deeper renewable generation in insular energy systems. Renew Sustain Energy Rev 2016;53:163–77.
[15] Bevrani H, Watanabe M, Mitani Y. Power system monitoring and control. John Wiley & Sons; 2014.
[16] Bevrani H, Ise T, Miura Y. Virtual synchronous generators: A survey and new perspectives. Int J Electr Power Energy Syst 2014;54:244–54.
[17] Dreidy M, Mokhlis H, Mekhilef S. Inertia response and frequency control techniques for renewable energy sources: a review. Renew Sustain Energy Rev 2017;69:144–55.
[18] Luo X, Wang J, Dooner M, Clarke J. Overview of current development in electrical energy storage technologies and the application potential in power system operation. Appl Energy 2015;137:511–36.
[19] Arani AAK, Karami H, Gharehpetian GB, Hejazi MSA. Review of Flywheel Energy Storage Systems structures and applications in power systems and microgrids. Renew Sustain Energy Rev 2017;69:9–18.
[20] Tielens P, Van Hertem D. The relevance of inertia in power systems. Renew Sustain Energy Rev 2016;55:999–1009.
[21] Gonzalez-Longatt F, Bonfiglio A, Procopio R, Bogdanov D. Practical limit of synthetic inertia in full converter wind turbine generators: simulation approach. Electrical Apparatus and Technologies (SIELA), 2016 19th International Symposium on: IEEE; 2016. p. 1–5.
[22] Ma J, Qiu Y, Li Y, Zhang W, Song Z, Thorp JS. Research on the impact of dfig virtual inertia control on power system small-signal stability considering the phase-locked loop. IEEE Trans Power Syst 2017;32:2094–105.
[23] Mu Y, Wu J, Ekanayake J, Jenkins N, Jia H. Primary frequency response from electric vehicles in the great britain power system. IEEE Trans Smart Grid 2013;4:1142–50.
[24] Hirase Y, Abe K, Sugimoto K, Shindo Y. A grid-connected inverter with virtual synchronous generator model of algebraic type. Electr Eng Japan 2013;184:10–21.
[25] Iqbal F, Khan MT, Siddiqui AS. Optimal placement of DG and DSTATCOM for loss reduction and voltage profile improvement. Alex Eng J 2017 [in press].
[26] Mohanty A, Viswavandya M, Mishra DK, Ray PK, Pragyan S. Modelling & simulation of a PV based micro grid for enhanced stability. Energy Procedia 2017;109:94–101.
[27] Hirase Y, Noro O, Yoshimura E, Nakagawa H, Sakimoto K, Shindo Y. Virtual synchronous generator control with double decoupled synchronous reference frame for single-phase inverter. IEEJ J Indus Appl 2015;4:143–51.
[28] Sakimoto K, Sugimoto K, Shindo Y, Ise T. Virtual synchronous generator without phase locked loop based on current controlled inverter and its parameter design. IEEJ Trans Power Energy 2015;135:462–71.
[29] D'Arco S, Suul JA, Fosso OB. A virtual synchronous machine implementation for distributed control of power converters in smartgrids. Electr Power Syst Res 2015;122:180–97.
[30] Lu L-Y, Chu C-C. Consensus-based secondary frequency and voltage droop control of virtual synchronous generators for isolated AC micro-grids. IEEE J Emerg Select Top Circ Syst 2015;5:443–55.
[31] Rongliang S, Xing Z, Liu F, Haizhen X, Chao H, Yong Y, et al. Research on power compensation strategy for diesel generator system based on virtual synchronous generator. In: 2016 IEEE 8th international power electronics and motion control conference (IPEMC-ECCE Asia); 2016. p. 939–43.
[32] Liu J, Miura Y, Ise T. Comparison of dynamic characteristics between virtual synchronous generator and droop control in inverter-based distributed generators. IEEE Trans Power Electron 2016;31:3600–11.
[33] Hirase Y, Sugimoto K, Sakimoto K, Ise T. Analysis of resonance in microgrids and effects of system frequency stabilization using a virtual synchronous generator. IEEE J Emerg Select Top Power Electr 2016;4:1287–98.
[34] Tang X, Deng W, Qi Z. Investigation of the dynamic stability of microgrid. IEEE Trans Power Syst 2014;29:698–706.
[35] Liu J, Miura Y, Bevrani H, Ise T. Enhanced virtual synchronous generator control for parallel inverters in microgrids. IEEE Trans Smart Grid 2017 [in press].
[36] Hirase Y, Abe K, Noro O, Sugimoto K, Sakimoto K. Stabilization effect of virtual synchronous generators in microgrids with highly penetrated renewable energies. In: 2016 IEEE 17th workshop on control and modeling for power electronics (COMPEL); 2016. p. 1–8.
[37] Shintai T, Miura Y, Ise T. Oscillation damping of a distributed generator using a virtual synchronous generator. IEEE Trans Power Delivery 2014;29:668–76.
[38] Xiong L, Zhuo F, Wang F, Liu X, Chen Y, Zhu M, et al. static synchronous generator model: a new perspective to investigate dynamic characteristics and stability issues of grid-tied PWM inverter. IEEE Trans Power Electron 2016;31:6264–80.
[39] Soni N, Doolla S, Chandorkar MC. Inertia design methods for islanded microgrids having static and rotating energy sources. IEEE Trans Ind Appl 2016;52:5165–74.
[40] Zhong QC, Konstantopoulos GC, Ren B, Krstic M. Improved synchronverters with bounded frequency and voltage for smart grid integration. IEEE Transactions on Smart Grid 2017 [in press].
[41] Serban I, Ion CP. Microgrid control based on a grid-forming inverter operating as virtual synchronous generator with enhanced dynamic response capability. Int J Electr Power Energy Syst 2017;89:94–105.
[42] Bevrani H. Robust power system frequency control. Springer; 2014.
[43] Anderson PM, Fouad AA. Power system control and stability. John Wiley & Sons; 2008.

Please cite this article in press as: Hirase Y et al. A novel control approach for virtual synchronous generators to suppress frequency and voltage fluctuations in microgrids. Appl Energy (2017), http://dx.doi.org/10.1016/j.apenergy.2017.06.058